ACS APPLIED MATERIALS & INTERFACES

Research Article

Cite This: ACS Appl. Mater. Interfaces 2019, 11, 19260−19266

www.acsami.org

Optical Properties of $In_{2x}Ga_{2-2x}O_3$ Nanowires Revealed by Photoacoustic Spectroscopy

Szymon J. Zelewski,*[,†] Ziyao Zhou,[‡,§] Fangzhou Li,[‡] Xiaolin Kang,[‡] You Meng,[‡] Johnny C. Ho,*[,‡,§] and Robert Kudrawiec*[,†]

[†]Faculty of Fundamental Problems of Technology, Wrocław University of Science and Technology, Wybrzeże Wyspiańskiego 27, 50-370 Wrocław, Poland

[‡]Department of Materials Science and Engineering, City University of Hong Kong, 83 Tat Chee Avenue, Kowloon, Hong Kong SAR, P. R. China

[§]Shenzhen Research Institute, City University of Hong Kong, Shenzhen 518057, P. R. China

Supporting Information

ABSTRACT: Group III oxides, such as In_2O_3 and Ga_2O_3, have proved to be good candidates as active materials for novel electronic devices, including high-mobility transistors, gas sensors, and UV photodetectors. The ability to tune optical and electronic properties is provided by alloying $In_{2x}Ga_{2-2x}O_3$ (InGaO) in a broad compositional range. Further development of InGaO compounds in the form of nanowires (NWs) would overcome the technological limitations, such as the substrate crystal lattice mismatch and the inability to fabricate high quality structures above the critical thickness. In this work, optical properties of alloyed InGaO NWs in a wide compositional range are carefully assessed. Unlike classical optical characterization methods, photoacoustic spectroscopy reveals the fundamental absorption edge despite the strong light scattering in porous and randomly oriented nanowires structure. An unusual compositional band gap dependence is also observed, giving insight into the phase segregation effect and increased quality of mixed NWs. In addition, photoacoustic measurements disclose potential applications of InGaO NWs in remote, light-driven loudspeakers because of intense photoacoustic effect in nanowire ensembles in this material system.

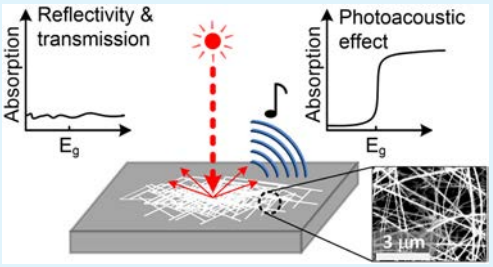

KEYWORDS: *In_2O_3, Ga_2O_3, InGaO, nanowire, photoacoustic spectroscopy*

INTRODUCTION

Group III oxides (e.g., In_2O_3, Ga_2O_3 and their alloys of $In_{2x}Ga_{2-2x}O_3$, InGaO) are wide band gap semiconductors (3−5 eV) covering UV-A to UV-C ranges.[1,2] Even though these thin film materials have already been widely explored for various technological applications, including the resistive oxygen sensors and others,[3] advanced preparation in the form of nanowires (NWs) would further lead to the realization of many novel devices, such as high electron mobility field-effect transistors (FETs)[4,5] and highly efficient solar-blind photodetectors.[6−9] Controlled anisotropy and large surface-to-volume ratio typically serve as the specific attributes facilitating all high-performance nanostructured devices. These NWs would also enable the effective device integration with silicon-based technology since the growth of crystalline NWs here is not restricted by any lattice mismatch issue of the underlying substrate and, hence, overcoming the notorious critical thickness limitation of other epitaxial nanostructures.

In general, the mixed compounds of In_2O_3 and Ga_2O_3 are scientifically interesting because this semiconductor alloying technique with varying In and Ga concentrations in $In_{2x}Ga_{2-2x}O_3$ is a well-known method for reliably tuning the band gap energy, which can directly manipulate the optical and electrical properties of the materials. It is also noted that the local atomic aggregation and crystal defect formation would significantly deteriorate physical properties of the alloy compounds; therefore, it is essential to accurately characterize the materials to further optimize their growth and processing methods for the enhanced properties. For instance, the improved electron mobility has been obtained in alloyed InGaO NW FETs as compared to the devices made of pure In_2O_3 NWs because of the diminished density of oxygen vacancies.[10] Despite it being crucial to evaluate the optical properties of NWs for the design of advanced optoelectronic devices, the literature reports mostly focus on pure In_2O_3 and Ga_2O_3 NWs with limited information about their alloys of $In_{2x}Ga_{2-2x}O_3$. Density functional theory calculations exhibited the different composition dependence of their energy band gap of monoclinic and cubic bixbyite InGaO crystals.[11] Experimental data revealed the linear dependence for compounds with the high Ga content suggesting the monoclinic structure, while supporting the parabolic dependence for In-rich

Received: January 13, 2019
Accepted: May 10, 2019
Published: May 10, 2019

DOI: 10.1021/acsami.9b00756
ACS Appl. Mater. Interfaces 2019, 11, 19260−19266

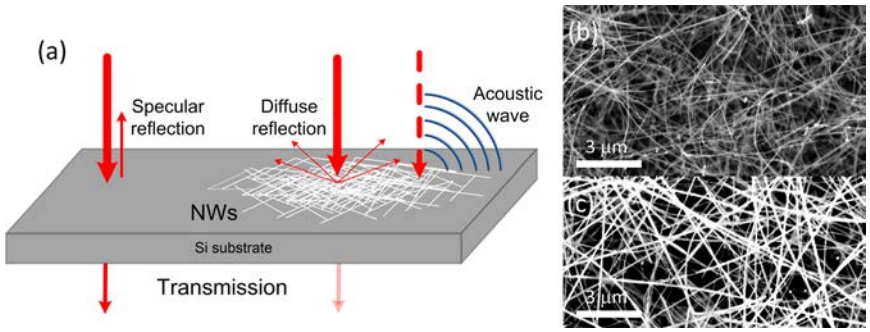

Figure 1. Schematic of optical effects in the surrounding of semiconductor nanowires (a), SEM images of pure Ga_2O_3 (b), and InGaO (precursor In and Ga mixing ratio of 1:1) nanowires grown on the Si substrate (c).

compounds with a bowing parameter of 3.18 eV. According to the same theoretical study, the fundamental transition was supposed to be forbidden with a smaller bowing parameter, which led to a large difference of ∼0.75 eV between the allowed and dark states in pure In_2O_3. In this regard, there have been few experimental studies assessing the band gap and their corresponding information about $In_{2x}Ga_{2-2x}O_3$ using optical transmission,[12,13] photoconductivity,[13] diffuse reflectance,[14] and ellipsometry[15] for an in-depth understanding.

To the best of our knowledge, until now, there is no study available on the optical absorption of alloyed InGaO NWs. One probable reason could be that the technicalities of conventional optical spectroscopic methods make it difficult to characterize NWs properly. At the same time, since NWs may contribute the substantial difference to their optical properties as compared with the bulk 3D counterparts, such as the possible quantum confinement size effect leading to the blue-shift of their band gap, it is necessary to accurately evaluate their optical properties. In particular, information about their compositional band gap behavior is important for validating the materials' usefulness, implicitly in electronic devices for maximizing the on/off current ratio of FETs and explicitly in photosensors and photovoltaic cells to enhance the device efficiency.

In this work, we demonstrate the use of photoacoustic spectroscopy to reveal the unique optical properties of randomly oriented and crystalline $In_{2x}Ga_{2-2x}O_3$ NWs, spanning the value of x all the way from 0 (Ga_2O_3) to 1 (In_2O_3). Utilizing the photoacoustic method, direct measurements of the light absorption characteristics of NWs with neglecting the scattering effect would give a powerful alternative to resolve the issues of conventional transmission and reflectance techniques. Importantly, the obtained spectra of $In_{2x}Ga_{2-2x}O_3$ as well as pure Ga_2O_3 and In_2O_3 NWs can effectively lead to the determination of their band gap energies along with understanding the effect of phase segregation in InGaO on the optical response of NW ensembles. All these findings indicate evidently the promising potency of using remote sound generation arose from the intense photoacoustic signals from NWs, which can provide valuable optical properties of nanostructures that are not easily assessed by other techniques.

RESULTS AND DISCUSSION

Figure 1a shows a schematic of optical effects occurring around the investigated structures. While illuminating a bare silicon substrate, the incident light is specularly reflected, with intensity depending on the surface quality. A small part of the light is also transmitted; however, the product αd, where α is the optical absorption coefficient and d is the sample thickness, in the case of typical substrates with $d > 100$ μm exceeds the optimal value of 1 near the fundamental band gap, causing sample opaqueness. Being wide-gap semiconductors, In_2O_3 and Ga_2O_3 in their bulk form are transparent to visible light.[16] In contrast, the investigated nanowires form white and porous structure on top of the substrate, suggesting strong light scattering. Scanning electron microscope (SEM) images shown in Figure 1b,c reveal random, net-like orientation of nanowires. As shown in the transmission electron microscope (TEM) image in Figure S1a, the representative $In_{1.8}Ga_{0.2}O_3$ NW has a thin diameter of 28 nm. The crystalline nature of the $In_{1.8}Ga_{0.2}O_3$ NW is evidenced by the SAED patterns. In specific, the clear lattice spacing of $In_{1.8}Ga_{0.2}O_3$ NW is measured to be ∼2.5 Å, corresponding to the {400} planes of cubic In_2O_3, further confirming the decent crystallinity of the NW. As seen in the XRD pattern of the same sample (Figure S2), all the diffraction peaks can be indexed to cubic In_2O_3 (JCPDS Card No. 06-0416), suggesting the phase purity of Ga-doped In_2O_3 NWs. The diffuse-dominated reflection from the sample surface hinders the ability to obtain intrinsic transmission spectrum of nanowires, following the standard procedure for determining optical absorption and material band gap. The combination of substrate opaqueness and light scattering makes it desirable to look for alternative, non-destructive characterization methods in studies of nanowires.

Photoacoustic and photothermal methods are known to be insensitive to scattered light, since the generated signal is proportional to the optical absorption coefficient of the investigated material.[17] When excited with a modulated light beam from the top side, the absorption causes periodic pressure changes inside the measurement cell, i.e., acoustic waves of frequency equal to the modulation frequency. The technical advantages of photoacoustic spectroscopy have been used in determining optical spectra of semiconducting nanowires,[18,19] quantum dots,[20,21] and other challenging structures, including powdered or amorphous materials, fluorescent compounds, 2D layered semiconductors,[22−26] or biological samples.[27] In addition, time- and frequency-resolved measurements of the photoacoustic signal can also be used to obtain thermal and carrier transport properties of materials, including thermal diffusivity and conductivity,[28] nonradiative lifetimes, and carrier diffusion coefficient.[29,30] Recent advances in contactless determination of thermal conductivity by means of photoacoustic and photothermal methods[31−33] pave the way for further studies of emerging electronic nanostructures[34−37] and thermoelectric materials.[38−40]

DOI: 10.1021/acsami.9b00756
ACS Appl. Mater. Interfaces 2019, 11, 19260−19266

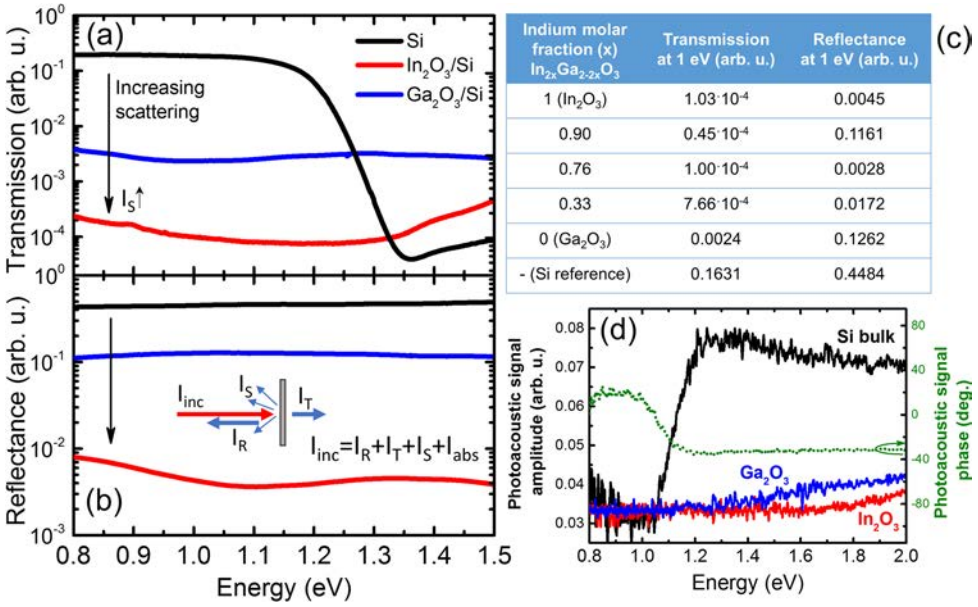

Indium molar fraction (x) $In_{2x}Ga_{2-2x}O_3$	Transmission at 1 eV (arb. u.)	Reflectance at 1 eV (arb. u.)
1 (In_2O_3)	$1.03 \cdot 10^{-4}$	0.0045
0.90	$0.45 \cdot 10^{-4}$	0.1161
0.76	$1.00 \cdot 10^{-4}$	0.0028
0.33	$7.66 \cdot 10^{-4}$	0.0172
0 (Ga_2O_3)	0.0024	0.1262
- (Si reference)	0.1631	0.4484

Figure 2. Representative room temperature transmission (a) and reflectance (b) spectra of reference Si substrate and pure In_2O_3/Ga_2O_3 nanowires, a summary of quantitative analysis supporting the prediction of strong light scattering by nanowires (c), and a comparison of photoacoustic spectra of the investigated materials (d).

In principle, wide-gap material nanostructures deposited on macroscopically thick Si substrate necessary for proper device assembly cannot be probed by classic optical spectroscopy. The transmitted light intensity has to drop after passing the Si band gap, leaving the system insensitive to any absorption features occurring at higher photon energies. To verify this hypothesis, we show a comparison of room temperature optical transmission (Figure 2a) and reflectivity (Figure 2b) spectra of pure In_2O_3/Ga_2O_3 nanowires grown on a Si substrate and a clean substrate for reference. The thick, pristine silicon is transparent in the infrared range up to ∼1.1 eV when it starts absorbing light, leading to a rapid decrease in the transmitted light intensity, in agreement with the indirect band gap of crystalline Si. Corresponding transmission measurements of nanowires grown on a Si substrate reveal significantly smaller signal with no characteristic features in the spectral region of interest. In the case of Ga_2O_3/Si, the below-gap transmission decrease ratio with respect to the clean substrate reaches 65. At energies above 1.3 eV it seems that the Ga_2O_3 sample becomes more transparent than the reference substrate indicating weaker absorption, but the calculation of optical absorption involves the reflectivity which is the strongest for bare Si substrate. For In_2O_3 nanowires sample the diminishment of optical response is even stronger, with an order of magnitude cut in transmission and reflectivity as compared to Ga_2O_3. This observation coincides with higher volume of the material deposited on top of the substrate (see a photograph of the samples in Figure S3) and supports the prediction of strong influence of light scattering in classic optical spectroscopy experiments. It is important to note that macroscopic transmission and reflectivity measurements are sensitive to any local roughness which add up affecting the response within the probing light spot.

The same procedure was applied to mixed InGaO nanowires. The table in Figure 2c summarizes the quantitative analysis taking the optical transmittance and reflectivity at 1.0 eV, an energy chosen assuming negligible contribution of band gap absorption to light extinction. Among the studied samples, the relative loss in transmission is more substantial than in reflectivity with a difference of 2 orders of magnitude in the extreme cases.

To confront the obtained results, we performed photoacoustic measurements on the same set of samples. The spectra shown in Figure 2d reveal the common below-gap photoacoustic signal for reference Si and Ga_2O_3/In_2O_3 nanowires. Its value is recognized as the background level inside the measurement cell coming from the absorption of the cell walls and transmission window as well as the intrinsic noise of the system. The amplitude spectrum of the reference Si substrate exhibits an absorption edge in the 1.05−1.20 eV range, saturating at higher energies. The band-gap-related origin of the measured signal is confirmed by the phase shift in the same spectral region, attributed to the heat wave caused by periodic temperature oscillations near the sample surface.

The spectra of In_2O_3 and Ga_2O_3 nanowires remain flat up to 2.0 eV, showing no absorption coming from the Si substrate. This result expands our previous findings on GaAs/GaAsBi core−shell nanowires,[18] where the substrate-related signal is significant at low modulation frequencies and can be reduced by tuning the frequency up to the thermally thick limit, when the thermal diffusion length is comparable with the sample thickness. We assign these differences to distinct arrangement of nanowires. As opposed to perpendicularly oriented (normal to the substrate surface) GaAsBi nanowires studied previously, InGaO ones promote strong light scattering before reaching the substrate surface due to random orientation and higher filling factor.

Broadband photoacoustic spectra of pure In_2O_3, Ga_2O_3, and mixed $In_{2x}Ga_{2-2x}O_3$ nanowires are presented in Figure 3. The absorption dependence is relatively flat in the visible range, with a small bump around 2.4 eV interpreted as defect-related absorption (see the inset). For pure In_2O_3, at photon energies of ∼2.7 eV the photoacoustic signal amplitude rapidly increases, revealing a fundamental absorption edge and drawing the low-energy optical response limit for selected compounds. A broad shoulder forms in the 3.2−3.6 eV range,

DOI: 10.1021/acsami.9b00756
ACS Appl. Mater. Interfaces 2019, 11, 19260−19266

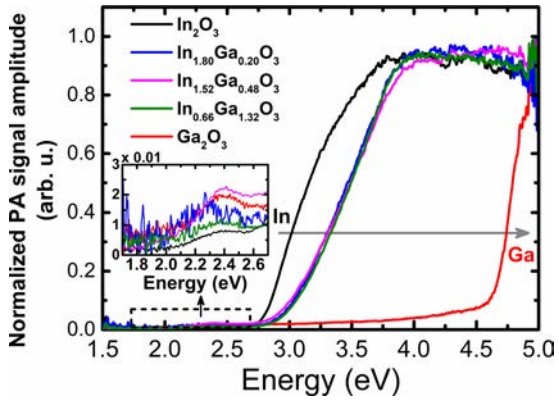

Figure 3. Photoacoustic spectra of pure and mixed $In_{2x}Ga_{2-2x}O_3$ nanowires with different stoichiometry. The inset shows zoomed-in low-energy absorption.

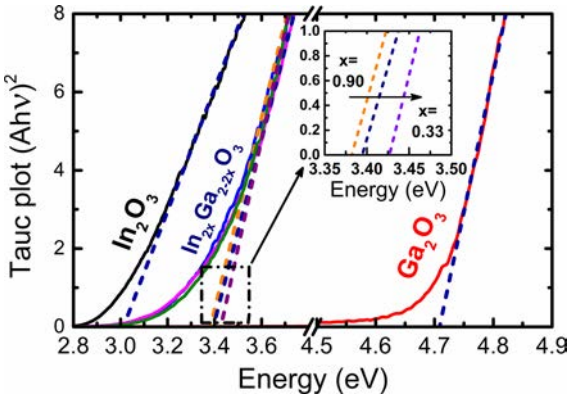

Figure 4. Tauc plots for direct allowed transition used to determine band gap energies of In_2O_3, Ga_2O_3, and alloyed InGaO nanowires. The inset zooms in the small energetic shift region of mixed InGaO compounds.

when eventually the signal saturates at a constant value. A similar behavior is observed on pure Ga_2O_3 in deep ultraviolet, with steeper edge and no saturation due to limited measurement system sensitivity when approaching 5.0 eV. The spectra of mixed InGaO nanowires fit between pure In_2O_3 and Ga_2O_3, very close to each other regardless of the stoichiometry. This effect can be explained by phase segregation of In_2O_3 and Ga_2O_3 within nanowires, possible for alloys with Ga content exceeding 10%.[10] In such a case, the In_2O_3 absorption is expected to be dominant in the optical spectrum. The 200 meV blue-shift of the observed optical gap might result from decreased defect-related absorption of O_2 vacancies as a consequence of higher Ga−O atomic binding energy. To support this claim, we performed X-ray photoelectron spectroscopy on mixed InGaO NWs, shown in Figure S4. The component labeled as O_H located at 532.15 eV, with a higher binding energy, is usually attributed to the presence of loosely bound oxygen (e.g., H_2O or O_2) on the surface of NWs. The medium binding energy component at 530.8 eV, labeled as O_M, is related to the O^{2-} ions that are in the oxygen-deficient regions. The component at the lower binding energy (529.5 eV), labeled as O_L, represents the O^{2-} ions located in the In_2O_3 lattice. The area ratio of O_L/O_M in $In_{1.8}Ga_{0.2}O_3$ NWs was determined to be 2.4, which is larger than that of pure In_2O_3 NWs (e.g., 1.4; as reported in our recent paper[9]). Because the Ga−O bonds typically have larger bond energies (353.5 kJ/mol) than that of In−O bonds (320.1 kJ/mol), the Ga incorporation in In_2O_3 NWs can improve the effectiveness of oxygen bonding with metal constituents and hence decrease the density of oxygen vacancies.

The standard Tauc plot analysis was performed to determine band gap energies from photoacoustic spectra. Assuming the direct character of the fundamental band gap, $(Ah\nu)^2$ is plotted versus the excitation photon energy (Figure 4). All processed traces are well approximated with a linear function ($R^2 > 0.99$). By extrapolating the fitted lines to zero, the band gap energy is taken at the intercept point.

Band gaps of In_2O_3 and Ga_2O_3 are determined to be 3.01 ± 0.02 and 4.71 ± 0.02 eV, respectively. The value for Ga_2O_3 agrees well with the original transmission spectroscopy result on a single crystal (4.7 eV).[2] Both there and in our work unpolarized light was used in the optical setup. Further studies show that the use of linearly polarized beam oriented toward different crystallographic axes gives absorption edges varying from 4.54 to 4.90 eV.[41] A shoulder at 4.65 eV was observed in some orientations, coinciding with a transition seen in the reflectivity spectrum measured with the electric vector parallel to the *c*-axis. In the case of In_2O_3, the band gap nature is intensively discussed in the literature. Early studies show an absorption edge at 3.75 eV corresponding to a direct allowed transition, with supposed indications of the presence of an indirect gap at much lower energies reaching 2.619 eV.[42] X-ray spectroscopy reports confirmed the direct fundamental gap character, with a conduction band elevated by 2.9 eV above the valence band minimum at the Γ point of the Brillouin zone.[43] Another report contains band gap determination from detailed optical measurements on cubic and rhombohedral In_2O_3 crystals, with a gap difference of 90 meV between the two phases.[1] Our result matches both band gaps within the uncertainty, with the absolute value almost identical to the one reported for the rhombohedral phase (3.02 eV). Even though the authors determined the band gaps from the weak absorption tail, our spectra reveal a strong absorption edge in this region. This effect can be explained by high sensitivity of photoacoustic measurements to low optical absorption coefficients, often surpassing the abilities of transmission spectroscopy. The agreement of our band gap energies with literature values for bulk crystals suggests the lack of quantum confinement in the studies nanowires, with the smallest dimension (the nanowire diameter) larger than the quantization limit.

Band gaps of alloyed InGaO nanowires are ∼400 meV higher than for pure In_2O_3, spread over a range of only 50 meV (from 3.38 to 3.43 eV) despite big stoichiometric differences. The band gap increases with the Ga content, following the expected trend. Such small changes in the compositional band gap dependence cannot be explained by flattening caused by the bowing parameter, held true only for high In contents.[11] In the proposed interpretation we state that the In_2O_3/Ga_2O_3 phase separation leads to dominating contribution of In_2O_3 in the measured absorption. The significant blue-shift might originate from a simple fact of smaller In/Ga volumetric ratio. The band gap energies determined in our analysis compared with literature values are summarized in Figure 5.

Figure 6 shows room temperature photoluminescence (PL) spectra of the investigated nanowires compared with their Tauc plots to study the Stokes shift. For pure In_2O_3 and Ga_2O_3 the spectra consist of one broad (fwhm of ∼500 meV) peak, located at 2.15 eV (576 nm) and 3.18 eV (390 nm),

DOI: 10.1021/acsami.9b00756
ACS Appl. Mater. Interfaces 2019, 11, 19260−19266

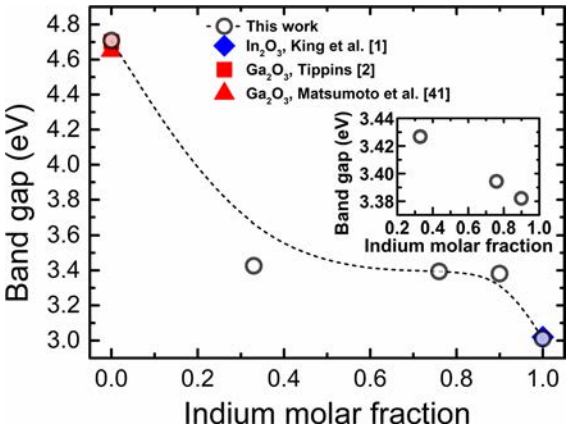

Figure 5. Summary of the determined band gap energies of pure and alloyed $In_{2x}Ga_{2-2x}O_3$ nanowires (x being the Indium molar fraction), including the compositional dependence. The dashed line is a guide to the eye. Additional points represent the literature data for selected compounds.

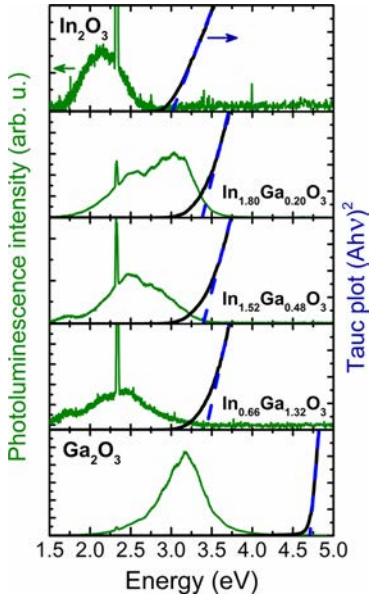

Figure 6. Room temperature photoluminescence spectra plotted with absorption edges of pure and alloyed InGaO nanowires. The sharp feature at 2.33 eV is an artifact arising from scattered light of a residual second harmonic present in the 1064 nm pumped excitation laser beam.

respectively. The emission intensity is the strongest for the Ga_2O_3 sample, almost covering up an experimental artifact present at 532 nm (2.33 eV) in the other spectra. For mixed InGaO nanowires, an exceptionally broad emission covering the green and blue spectral range occurs, most likely arising from two separate peaks. In all cases the PL emission is located at lower energies than the absorption, with no signs of band edge recombination. The blue emission is typically assigned to the donor level of oxygen vacancies;[44−46] however, another explanation based on the strong electron−phonon coupling was recently proposed for the big red-shift of PL emission in bulk Ga_2O_3.[47] For a better understanding of the PL spectra from the nanowire ensemble it would be interesting to study PL from individual nanowires and correlate these spectra with their local structural properties, which is planned as further work.

The spectra shown in Figure 3 are corrected with respect to the reference spectrum of the setup and normalized to the maximum value in the saturation region. It is worth mentioning that the absolute photoacoustic signal intensities obtained on mixed InGaO nanowires in the saturated part of the spectrum exceed the intensity of the reference spectrum, reaching relative values as high as 4. Strong evidence for robust nonradiative energy transfer in the form of the photoacoustic effect was also noticed during photoluminescence measurements. Upon sample illumination with a pulsed laser at the repetition rate of 1 kHz a distorted, audible sound could be heard near the sample, even without enclosing it and using special measurement equipment. A demonstration of acoustic waves generation inside the measurement cell while illuminating the sample with a 213 nm laser is shown in Video S1, with the output signal taken directly from the measurement microphone. Intense photoacoustic conversion was recently reported on graphene foam,[48] leading to a proof-of-concept remotely driven, wireless loudspeaker. Our observation strongly suggests that nanowires, treated as porous nanostructures, could also be considered for such applications.

CONCLUSIONS

Photoacoustic spectroscopy was demonstrated as an alternative and powerful tool for determining optical properties of porous, randomly ordered NWs, which overcame the light scattering effect limiting the usefulness of classic reflectivity and transmission measurements. Band gaps of pure In_2O_3 and Ga_2O_3 NWs determined from Tauc plots of amplitude photoacoustic spectra agree very well with literature values for their bulk counterparts. The first observation of small compositional band gap dependence of alloyed $In_{2x}Ga_{2-2x}O_3$ NWs is reported, attributed to the phase segregation causing the dominating contribution of In_2O_3 in absorption spectra. Broadening of the photoluminescence spectra of alloyed $In_{2x}Ga_{2-2x}O_3$ NWs confirms the phase segregation effect. Possible applications in remote sound generation arise from intense photoacoustic effect in the investigated NWs because of efficient nonradiative energy transfer. The presented approach to optical characterization of NWs by photoacoustic spectroscopy paves the way for further studies of porous structures, metamaterials, and other challenging systems.

EXPERIMENTAL SECTION

Nanowires Growth and Characterization. Si/SiO_2 (50 nm thick thermally grown oxide) substrates with a layer of 0.1 nm (nominal thickness) Au film predeposited by thermal evaporation was used for the growth of NWs by a typical CVD method. For the growth of pure In_2O_3 and Ga_2O_3 NWs, high purity 1.5 g of In or Ga metal granules (1−2 mm in size; 99.999% in purity; China Rare Metal) was used as the In or Ga source. For the growth of InGaO NWs, the metal granules of both Ga and In (1−2 mm in size; 99.999% in purity; China Rare Metal) were used as the In and Ga source materials with different mixing ratios (e.g., 3:1, 1:1, and 1:3; 1.5 g in total) to control the stoichiometry of the NWs. Also, 0.5 g of graphite powder (<20 μm in size, synthetic; Sigma-Aldrich) was mixed with metal source as the precursor. A small quartz tube (10 cm in length and 1 cm in diameter) with precursor mixture in the sealed end and substrate in the open end was used as the container for the growth. The entire setup was then placed at the center of a large quartz tube (1 in. in diameter), which was located in a single-zone horizontal tube furnace. Next, a mixed gas of oxygen (99.999% in purity) and argon (99.9995% in purity) with a volume ratio of 4:96 was introduced into the quartz tube, which acted as carrier gas and provided oxygen for the reaction. The temperature for the synthesis

DOI: 10.1021/acsami.9b00756
ACS Appl. Mater. Interfaces 2019, 11, 19260−19266

was 1040 °C with a holding time of 30 min, and the heating rate was about 30−35 °C/min. Eventually, the fluffy white product could be found on the substrate. Afterward, the NW morphologies were examined using scanning electron microscope (SEM, XL30, FEI). The crystal structure and crystallinity of the obtained NWs were determined by collecting XRD pattern on a Philips powder diffractometer and imaging with a high-resolution transmission electron microscope (HRTEM, JEOL 2100F). To prepare the TEM samples, NWs were first suspended in high-purity anhydrous ethanol solution and then drop-casted on a Cu grid. The chemical state of the as-prepared NWs was examined by X-ray photoelectron spectroscopy (XPS, ULVAC-PHI 5802).

Photoacoustic Spectroscopy. The microphone detection configuration was used for photoacoustic measurements. The samples were mounted inside a cylindrical aluminum cell sealed with a quartz transmission window. The light beam from a 450 W xenon arc lamp (ozone-free Osram XBO450) was modulated with a mechanical chopper at 40 Hz, dispersed with a Czerny−Turner grating monochromator (Horiba iHR, 320 mm focal length, 1800 grooves/mm ruled grating), and focused on the sample surface forming a spot of 1 mm × 2 mm in size. Acoustic waves generated inside the cell were detected by a 1/4 in. condenser electret microphone capsule, separated from the sample space with a funnel to minimize the parasitic signal coming from scattered light. Amplitude and phase components of the photoacoustic signal were measured with a lock-in amplifier (SRS SR830) at the time constant of 10 s. A thin layer of powdered carbon was used to obtain the reference spectrum for normalization. All measurements were performed at room temperature, using ambient air as the gas medium for acoustic wave propagation. To record Video S1 demonstrating the photoacoustic signal generation in $In_{1.80}Ga_{0.20}O_3$ nanowires, the same 213 nm laser as used for photoluminescence spectroscopy was used to excite the sample.

Photoluminescence Spectroscopy. A 213 nm pulsed nanosecond laser (CryLaS GmbH FQSS213-Q3-STA) with the average power of 3 mW was used as the excitation source. The photoluminescence collected in the backscattering mode was acquired with a compact Si CCD spectrophotometer (Ocean Optics HR4000) with a resolution of 1 nm.

Transmission and Reflectance Spectroscopy. A tunable light source consisting of a 150 W quartz tungsten halogen (QTH) lamp coupled with a monochromator (300 mm focal length) was used for optical transmission and reflectance measurements. Samples were mounted in the focal point of the beam. For transmission, the light passed through the sample was detected in the same optical axis, while for reflectance, the sample was tilted at a small angle to ensure near-normal incidence, allowing efficient light collection. An amplified InGaAs photodiode was used as a detector in both configurations.

■ ASSOCIATED CONTENT

Supporting Information

The Supporting Information is available free of charge on the ACS Publications website at DOI: 10.1021/acsami.9b00756.

Photograph of the studied samples, additional X-ray diffraction pattern, X-ray photoelectron spectra, high-resolution TEM images (PDF)

Video S1 showing the photoacoustic signal generation upon pulsed laser excitation of InGaO nanowires (AVI)

■ AUTHOR INFORMATION

Corresponding Authors

*(S.J.Z.) E-mail: szymon.zelewski@pwr.edu.pl.

*(J.C.H.) E-mail: johnnyho@cityu.edu.hk.

*(R.K.) E-mail: robert.kudrawiec@pwr.edu.pl.

ORCID

Szymon J. Zelewski: 0000-0002-6037-3701

Ziyao Zhou: 0000-0001-5313-1301

Fangzhou Li: 0000-0002-4722-8040

Xiaolin Kang: 0000-0002-9247-1875

You Meng: 0000-0002-5385-4080

Johnny C. Ho: 0000-0003-3000-8794

Robert Kudrawiec: 0000-0003-2593-9172

Author Contributions

S.J.Z., J.C.H., and R.K. conceived the project. S.J.Z., J.C.H., and R.K. prepared the manuscript. Z.Z. and F.L. grew the NWs. X.K. performed the SEM measurements, and Y.M. performed XRD, XPS, and TEM characterization. S.J.Z. performed and analyzed all optical measurements. All authors examined and commented on the manuscript.

Notes

The authors declare no competing financial interest.

■ ACKNOWLEDGMENTS

S.J.Z. acknowledges the support within the Etiuda 5 scholarship from National Science Centre Poland (No. 2017/24/T/ST3/00257). J.C.H. acknowledges the support from the General Research Fund of the Research Grants Council of Hong Kong SAR, China (No. CityU 11275916) and the National Natural Science Foundation of China (No. 51672229). The authors thank Prof. Kin Man Yu for initiating the project.

■ REFERENCES

(1) King, P. D. C.; Veal, T. D.; Fuchs, F.; Wang, Ch. Y.; Payne, D. J.; Bourlange, A.; Zhang, H.; Bell, G. R.; Cimalla, V.; Ambacher, O.; Egdell, R. G.; Bechstedt, F.; McConville, C. F. Band Gap, Electronic Structure, and Surface Electron Accumulation of Cubic and Rhombohedral In_2O_3. *Phys. Rev. B: Condens. Matter Mater. Phys.* **2009**, *79* (20), 205211.

(2) Tippins, H. H. Optical Absorption and Photoconductivity in the Band Edge of β − Ga_2O_3. *Phys. Rev.* **1965**, *140* (1A), A316−A319.

(3) Ogita, M.; Higo, K.; Nakanishi, Y.; Hatanaka, Y. Ga_2O_3 Thin Film for Oxygen Sensor at High Temperature. *Appl. Surf. Sci.* **2001**, *175-176*, 721−725.

(4) Chen, P.-C.; Shen, G.; Chen, H.; Ha, Y.; Wu, C.; Sukcharoenchoke, S.; Fu, Y.; Liu, J.; Facchetti, A.; Marks, T. J.; Thompson, M. E.; Zhou, C. High-Performance Single-Crystalline Arsenic-Doped Indium Oxide Nanowires for Transparent Thin-Film Transistors and Active Matrix Organic Light-Emitting Diode Displays. *ACS Nano* **2009**, 3 (11), 3383−3390.

(5) Zhang, H.; Meng, Y.; Song, L.; Luo, L.; Qin, Y.; Han, N.; Yang, Z.; Liu, L.; Ho, J. C.; Wang, F. High-Performance Enhancement-Mode Thin-Film Transistors Based on Mg-Doped In_2O_3 Nanofiber Networks. *Nano Res.* **2018**, *11* (3), 1227−1237.

(6) Feng, P.; Zhang, J. Y.; Li, Q. H.; Wang, T. H. Individual β-Ga_2O_3 Nanowires as Solar-Blind Photodetectors. *Appl. Phys. Lett.* **2006**, *88* (15), 153107.

(7) Li, Y.; Tokizono, T.; Liao, M.; Zhong, M.; Koide, Y.; Yamada, I.; Delaunay, J.-J. Efficient Assembly of Bridged β-Ga_2O_3 Nanowires for Solar-Blind Photodetection. *Adv. Funct. Mater.* **2010**, *20* (22), 3972−3978.

(8) López, I.; Castaldini, A.; Cavallini, A.; Nogales, E.; Méndez, B.; Piqueras, J. β-Ga_2O_3 Nanowires for an Ultraviolet Light Selective Frequency Photodetector. *J. Phys. D: Appl. Phys.* **2014**, *47* (41), 415101.

(9) Ouyang, W.; Teng, F.; He, J.-H.; Fang, X. Enhancing the Photoelectric Performance of Photodetectors Based on Metal Oxide Semiconductors by Charge-Carrier Engineering. *Adv. Funct. Mater.* **2019**, *29* (9), 1807672.

(10) Zhou, Z.; Lan, C.; Yip, S.; Wei, R.; Li, D.; Shu, L.; Ho, J. C. Towards High-Mobility $In_{2x}Ga_{2-2x}O_3$ Nanowire Field-Effect Transistors. *Nano Res.* **2018**, *11*, 5935.

(11) Peelaers, H.; Steiauf, D.; Varley, J. B.; Janotti, A.; Van de Walle, C. G. $(In_xGa_{1-x})_2O_3$ Alloys for Transparent Electronics. *Phys. Rev. B: Condens. Matter Mater. Phys.* **2015**, *92* (8), 085206.
(12) Oshima, T.; Fujita, S. Properties of Ga_2O_3-Based $(In_xGa_{1-x})_2O_3$ Alloy Thin Films Grown by Molecular Beam Epitaxy. *Phys. Status Solidi C* **2008**, *5* (9), 3113−3115.
(13) Vasyltsiv, V. I.; Rym, Ya. I.; Zakharko, Ya. M. Optical Absorption and Photoconductivity at the Band Edge of β-$Ga_{2-x}In_xO_3$. *Phys. Status Solidi B* **1996**, *195* (2), 653−658.
(14) Kudo, A.; Mikami, I. Photocatalytic Activities and Photophysical Properties of $Ga_{2-x}In_xO_3$ Solid Solution. *J. Chem. Soc., Faraday Trans.* **1998**, *94*, 2929−2932.
(15) Lee, K.-H.; Ok, K.-C.; Kim, H.; Park, J.-S. The Influence of Oxygen Partial Pressure on the Performance and Stability of Ge-Doped InGaO Thin Film Transistors. *Ceram. Int.* **2014**, *40* (2), 3215−3220.
(16) Tomm, Y.; Reiche, P.; Klimm, D.; Fukuda, T. Czochralski Grown Ga_2O_3 Crystals. *J. Cryst. Growth* **2000**, *220* (4), 510−514.
(17) Rosencwaig, A. Theoretical Aspects of Photoacoustic Spectroscopy. *J. Appl. Phys.* **1978**, *49* (5), 2905−2910.
(18) Zelewski, S. J.; Kopaczek, J.; Linhart, W. M.; Ishikawa, F.; Shimomura, S.; Kudrawiec, R. Photoacoustic Spectroscopy of Absorption Edge for GaAsBi/GaAs Nanowires Grown on Si Substrate. *Appl. Phys. Lett.* **2016**, *109* (18), 182106.
(19) Leahu, G.; Petronijevic, E.; Belardini, A.; Centini, M.; Li Voti, R.; Hakkarainen, T.; Koivusalo, E.; Guina, M.; Sibilia, C. Photo-Acoustic Spectroscopy Revealing Resonant Absorption of Self-Assembled GaAs-Based Nanowires. *Sci. Rep.* **2017**, *7* (1), 2833.
(20) Toyoda, T.; Yindeesuk, W.; Kamiyama, K.; Hayase, S.; Shen, Q. Effect of TiO_2 Crystal Orientation on the Adsorption of CdSe Quantum Dots for Photosensitization Studied by the Photoacoustic and Photoelectron Yield Methods. *J. Phys. Chem. C* **2014**, *118* (30), 16680−16687.
(21) Toyoda, T.; Yindeesuk, W.; Kamiyama, K.; Hayase, S.; Shen, Q. Adsorption and Electronic Structure of CdSe Quantum Dots on Single Crystal ZnO: A Basic Study of Quantum Dot-Sensitization System. *J. Phys. Chem. C* **2016**, *120* (30), 16367−16376.
(22) Ferreira da Silva, A.; Veissid, N.; An, C. Y.; Caetano de Souza, J.; Batista da Silva, A. V.; César Farias, P.; da Cruz, M. T. F. Optical Band Gap of the α−Mercuric Iodide. *J. Appl. Phys.* **1995**, *78* (9), 5822−5823.
(23) Ferreira da Silva, A.; Veissid, N.; An, C. Y.; Pepe, I.; Barros de Oliveira, N.; Batista da Silva, A. V. Optical Determination of the Direct Bandgap Energy of Lead Iodide Crystals. *Appl. Phys. Lett.* **1996**, *69* (13), 1930−1932.
(24) Witte, R. S.; Xin, H. Thermoacoustic and Photoacoustic Characterizations of Few-Layer Graphene by Pulsed Excitations. *Appl. Phys. Lett.* **2016**, *108* (14), 143104.
(25) Zelewski, S. J.; Kudrawiec, R. Photoacoustic and Modulated Reflectance Studies of Indirect and Direct Band Gap in van Der Waals Crystals. *Sci. Rep.* **2017**, *7* (1), 15365.
(26) Kopaczek, J.; Zelewski, S. J.; Polak, M. P.; Gawlik, A.; Chiappe, D.; Schulze, A.; Caymax, M.; Kudrawiec, R. Direct and Indirect Optical Transitions in Bulk and Atomically Thin MoS_2 Studied by Photoreflectance and Photoacoustic Spectroscopy. *J. Appl. Phys.* **2019**, *125* (13), 135701.
(27) Rosencwaig, A. Photoacoustic Spectroscopy of Solids. *Phys. Today* **1975**, *28* (9), 23−30.
(28) Hu, H.; Wang, X.; Xu, X. Generalized Theory of the Photoacoustic Effect in a Multilayer Material. *J. Appl. Phys.* **1999**, *86* (7), 3953−3958.
(29) Marín, E.; Riech, I.; Díaz, P.; Alvarado-Gil, J. J.; Baquero, R.; Mendoza-Alvarez, J. G.; Vargas, H.; Cruz-Orea, A.; Vargas, M. Photoacoustic Determination of Non-Radiative Carrier Lifetimes. *J. Appl. Phys.* **1998**, *83* (5), 2604−2609.
(30) Riech, I.; Gomez-Herrera, M. L.; Díaz, P.; Mendoza-Alvarez, J. G.; Herrera-Pérez, J. L.; Marín, E. Measurement of the Auger Lifetime in GaInAsSb/GaSb Heterostructures Using the Photoacoustic Technique. *Appl. Phys. Lett.* **2001**, *79* (7), 964−966.
(31) Singh, V.; Bougher, T. L.; Weathers, A.; Cai, Y.; Bi, K.; Pettes, M. T.; McMenamin, S. A.; Lv, W.; Resler, D. P.; Gattuso, T. R.; Altman, D. H.; Sandhage, K. H.; Shi, L.; Henry, A.; Cola, B. A. High Thermal Conductivity of Chain-Oriented Amorphous Polythiophene. *Nat. Nanotechnol.* **2014**, *9* (5), 384−390.
(32) Zhu, G.; Liu, J.; Zheng, Q.; Zhang, R.; Li, D.; Banerjee, D.; Cahill, D. G. Tuning Thermal Conductivity in Molybdenum Disulfide by Electrochemical Intercalation. *Nat. Commun.* **2016**, *7*, 13211.
(33) Li, S.; Zheng, Q.; Lv, Y.; Liu, X.; Wang, X.; Huang, P. Y.; Cahill, D. G.; Lv, B. High Thermal Conductivity in Cubic Boron Arsenide Crystals. *Science* **2018**, *361* (6402), 579−581.
(34) Ajayan, P.; Kim, P.; Banerjee, K. Two-Dimensional van Der Waals Materials. *Phys. Today* **2016**, *69* (9), 38−44.
(35) Manzeli, S.; Ovchinnikov, D.; Pasquier, D.; Yazyev, O. V.; Kis, A. 2D Transition Metal Dichalcogenides. *Nat. Rev. Mater.* **2017**, *2* (8), 17033.
(36) Alarawi, A.; Ramalingam, V.; Fu, H.-C.; Varadhan, P.; Yang, R.; He, J.-H. Enhanced Photoelectrochemical Hydrogen Production Efficiency of MoS_2-Si Heterojunction. *Opt. Express* **2019**, *27* (8), A352.
(37) Yip, S.; Shen, L.; Ho, J. C. Recent Advances in III-Sb Nanowires: From Synthesis to Applications. *Nanotechnology* **2019**, *30* (20), 202003.
(38) Kim, H.; Anasori, B.; Gogotsi, Y.; Alshareef, H. N. Thermoelectric Properties of Two-Dimensional Molybdenum-Based MXenes. *Chem. Mater.* **2017**, *29* (15), 6472−6479.
(39) Yang, L.; Chen, Z.-G.; Dargusch, M. S.; Zou, J. High Performance Thermoelectric Materials: Progress and Their Applications. *Adv. Energy Mater.* **2018**, *8* (6), 1701797.
(40) Jin, H.; Li, J.; Iocozzia, J.; Zeng, X.; Wei, P.-C.; Yang, C.; Li, N.; Liu, Z.; He, J. H.; Zhu, T.; Wang, J.; Lin, Z.; Wang, S. Hybrid Organic-Inorganic Thermoelectric Materials and Devices. *Angew. Chem.* **2019**, DOI: 10.1002/ange.201901106.
(41) Matsumoto, T.; Aoki, M.; Kinoshita, A.; Aono, T. Absorption and Reflection of Vapor Grown Single Crystal Platelets of β-Ga_2O_3. *Jpn. J. Appl. Phys.* **1974**, *13* (10), 1578−1582.
(42) Weiher, R. L.; Ley, R. P. Optical Properties of Indium Oxide. *J. Appl. Phys.* **1966**, *37* (1), 299−302.
(43) Walsh, A.; Da Silva, J. L. F.; Wei, S.-H.; Körber, C.; Klein, A.; Piper, L. F. J.; DeMasi, A.; Smith, K. E.; Panaccione, G.; Torelli, P.; Payne, D. J.; Bourlange, A.; Egdell, R. G. Nature of the Band Gap of In_2O_3 Revealed by First-Principles Calculations and X-Ray Spectroscopy. *Phys. Rev. Lett.* **2008**, *100* (16), 167402.
(44) Zhang, J.; Qing, X.; Jiang, F.; Dai, Z. A Route to Ag-Catalyzed Growth of the Semiconducting In_2O_3 Nanowires. *Chem. Phys. Lett.* **2003**, *371* (3−4), 311−316.
(45) Wang, F.; Han, Z.; Tong, L. Fabrication and Characterization of β-Ga_2O_3 Optical Nanowires. *Phys. E* **2005**, *30* (1−2), 150−154.
(46) Hadia, N. M. A.; Mohamed, H. A. Synthesis, Structure and Optical Properties of Single-Crystalline In_2O_3 Nanowires. *J. Alloys Compd.* **2013**, *547*, 63−67.
(47) Huynh, T. T.; Lem, L. L. C.; Kuramata, A.; Phillips, M. R.; Ton-That, C. Kinetics of Charge Carrier Recombination in β-Ga_2O_3 Crystals. *Phys. Rev. Mater.* **2018**, *2* (10), 105203.
(48) Giorgianni, F.; Vicario, C.; Shalaby, M.; Tenuzzo, L. D.; Marcelli, A.; Zhang, T.; Zhao, K.; Chen, Y.; Hauri, C.; Lupi, S. High-Efficiency and Low Distortion Photoacoustic Effect in 3D Graphene Sponge. *Adv. Funct. Mater.* **2018**, *28* (2), 1702652.

DOI: 10.1021/acsami.9b00756
ACS Appl. Mater. Interfaces 2019, 11, 19260−19266